Porosity Formation and Prevention in Pulsed Laser Welding

Jun Zhou
Department of Mechanical and Electrical Engineering Technology,
Georgia Southern University,
Engineering Technology Bldg., Room 1126,
232 Forest Drive,
Statesboro, GA 30460
e-mail: jzhou@georgiasouthern.edu

Hai-Lung Tsai
Department of Mechanical and Aerospace Engineering,
University of Missouri-Rolla,
207 Mechanical Engineering,
1870 Miner Circle,
Rolla, MO 65409
e-mail: tsai@umr.edu

Porosity has been frequently observed in solidified, deep penetration pulsed laser welds. Porosity is detrimental to weld quality. Our previous study shows that porosity formation in laser welding is associated with the weld pool dynamics, keyhole collapse, and solidification processes. The objective of this paper is to use mathematical models to systematically investigate the transport phenomena leading to the formation of porosity and to find possible solutions to reduce or eliminate porosity formation in laser welding. The results indicate that the formation of porosity in pulsed laser welding is caused by two competing factors: one is the solidification rate of the molten metal and the other is the backfilling speed of the molten metal during the keyhole collapse process. Porosity will be formed in the final weld if the solidification rate of the molten metal exceeds the backfilling speed of liquid metal during the keyhole collapse and solidification processes. Porosity formation was found to be strongly related with the depth-to-width aspect ratio of the keyhole. The larger the ratio, the easier porosity will be formed, and the larger the size of the voids. Based on these studies, controlling the laser pulse profile is proposed to prevent/eliminate porosity formation in laser welding. Its effectiveness and limitations are demonstrated in the current studies. The model predictions are qualitatively consistent with reported experimental results. [DOI: 10.1115/1.2724846]

Keywords: laser welding, modeling, heat transfer, fluid flow, pulse control, porosity formation, prevention

1 Introduction

Joining of components with high precision and small heat-affected zone has recently made laser welding more prevalent in industry. Especially, with large depth-to-width aspect ratio and high welding efficiency, keyhole mode laser welding is more promising when compared with conventional welding processes. However, in deep penetration laser welds, porosity is frequently observed [1–4]. Porosity deteriorates the strength of the welded part. In order to optimize the laser welding process and to ensure high weld quality and strength, it is necessary to understand how porosity is formed in the welding process and, subsequently, to find methods to reduce or eliminate porosity defects.

Over the years, some researchers have conducted experiments to investigate porosity formation in laser welding. Katayama et al. [5] studied porosity formation in welding A5083 alloy and 304 steel with a high power YAG laser. They reported that alot of pores/voids were formed due to the evaporation of metal from the bottom tip of the keyhole, with the vapor being trapped by the solidifying front. They also discovered that shielding gas was trapped in those pores/voids. Seto and co-workers [6] took x-ray transmission images of the keyhole dynamics during laser welding using a high-speed video camera. As shown in their images, the rear side of the molten metal was depressed near the bottom when the keyhole front was inclined in the rear direction at the root. The reflected laser beam can superheat the molten metal near the bottom, resulting in a depression due to the high recoil pressure acting on the molten metal. They concluded that the shape of the keyhole front had a significant influence on porosity formation. Katayama et al. [7] observed the fusion and solidification behavior of a molten puddle during laser spot welding of 316S steel. They found that the formation of porosity had a close correlation with the collapse of the keyhole right after the irradiation termination. Once the laser beam was terminated, the melt in the upper part of the keyhole flowed downward to fill the keyhole. Some gas seems to have been trapped in the lower part of the keyhole. At the same time, the upper part of the melt rapidly solidified, which prevented the melt from flowing to fill the keyhole. Thus porosity was formed in the weld.

Based on these experimental observations, several methods have been proposed to prevent porosity formation for keyhole mode laser welding. The first method [8] focused on preventing the invasion of shielding gas during the welding process by welding in a vacuum. The experimental results showed that in vacuum welding, evaporation of metals was intensive so that the metallic vapors swelled the middle and the bottom rear wall of the keyhole, but no pores or voids were generated in the rear or bottom part of the molten pool. However, welding in a vacuum environment is not feasible in most industrial situations because of its inflexibility and high cost. The second method is to use a particular kind of shielding gas that can be dissolved in the molten metal. In YAG and CO_2 laser welding of 304S steels [5,9], reduced porosity formation was found using the shielding gas N_2, compared to that using other shielding gases, due to the high solubility of N_2 in metals with a high Cr content. The use of CO_2 shielding gas to suppress porosity formation was also reported in YAG laser welding of mild steels [10]. However, this approach is only suitable for certain welding cases in which the shielding gas "matches" the weld metal, limiting its applications.

The last method is to control the flow of molten metal during the keyhole collapse process, allowing the lower part of the keyhole to be filled up by molten metal. This can be achieved by increasing the backfilling speed of the molten metal or by delaying the solidification of the molten metal. Delaying the solidification process can be realized by optimizing the pulse shape of the laser beam [7]. From experimental results, it was revealed that by adding a tailing power to the laser pulse, a deep keyhole weld without porosity could be produced. Since this method can be

Contributed by the Heat Transfer Division of ASME for publication in the JOURNAL OF HEAT TRANSFER. Manuscript received January 19, 2006; final manuscript received September 5, 2006. Review conducted by Ben Q. Li.

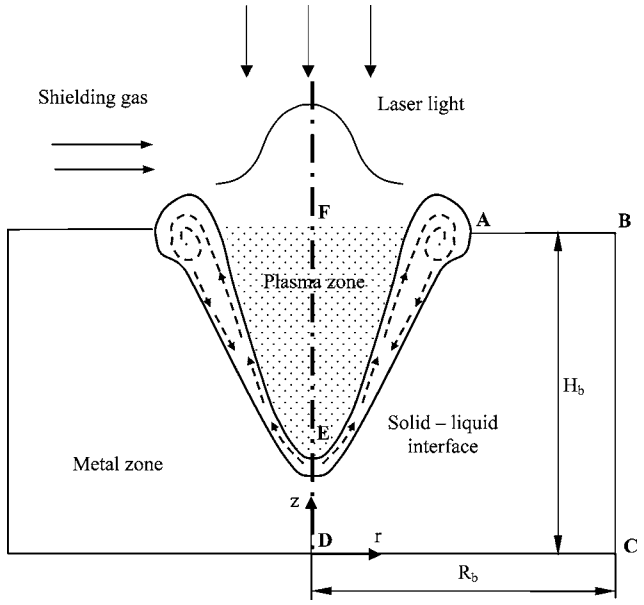

Fig. 1 Schematic sketch of a pulsed laser welding process

easily achieved compared with the aforementioned other methods, it is more practical to be adopted in industrial applications to prevent porosity formation.

So far, all reported research of porosity formation and prevention are based on experimental studies. Although experimental results such as the observations through microfocused x-ray transmission imaging can provide useful information about porosity formation, the underlying physics, such as temperature and velocity evolutions during the keyhole formation and collapse cannot be revealed. This is especially true for the phenomena that occur inside the keyhole. However, the temperature and velocity evolutions during the keyhole collapse and solidification processes have a significant influence on porosity formation. Hence, numerical simulation of keyhole mode laser welding is needed to study what happens during porosity formation. Until recently, a comprehensive numerical model was developed by Zhou et al. [11] to simulate the keyhole formation and collapse in the laser welding process. This work included the calculation of temperature field distributions, pressure balance, melt flow, free surface, laser-induced plasma, and multiple reflections. The model predictions are in good agreement with the experimental results. In this paper, this model is employed to systematically investigate the porosity formation mechanisms and the effectiveness of the prevention approach by optimizing the pulse shape in pulsed laser welding.

2 Mathematical Models

Figure 1 is a schematic sketch of stationary keyhole mode pulsed laser welding. The base metal is assumed to be 304S steel containing 100 ppm of sulfur. A finite difference model employing the volume of fluid (VOF) technique [12] and the continuum formulation [13] was used to calculate the momentum and energy transport in the keyhole and welding coupon. The VOF technique can handle a transient deformed weld pool surface, while the continuum formulation can handle fusion and solidification for the liquid region, the mush zone, and the solid region. Laser-induced plasma is often present in laser welding processes and it is a key factor affecting the keyhole dynamics. Due to the different energy transport mechanisms in the solid/liquid metal zone and the plasma zone, two submodels are developed to handle the transport phenomena in these two zones.

2.1 Metal Zone Simulation. The governing differential equations used to describe heat and mass transfer and fluid flow in a cylindrical coordinate (r-z system) given by Chiang and Tsai [13] are modified and used in the current study:

Continuity

$$\frac{\partial}{\partial t}(\rho) + \nabla \cdot (\rho \boldsymbol{V}) = 0 \tag{1}$$

Momentum

$$\frac{\partial}{\partial t}(\rho u) + \nabla \cdot (\rho \boldsymbol{V} u) = \nabla \cdot \left(\mu_l \frac{\rho}{\rho_l} \nabla u \right) - \frac{\partial p}{\partial r} - \frac{u_l}{K} \frac{\rho}{\rho_l}(u - u_s) - \frac{C\rho^2}{K^{0.5}\rho_l}|u - u_s|(u - u_s) - \nabla \cdot (\rho f_s f_l \boldsymbol{V}_r u_r) + \nabla \cdot \left(\mu_s u \nabla \left(\frac{\rho}{\rho_l} \right) \right) \tag{2}$$

$$\frac{\partial}{\partial t}(\rho v) + \nabla \cdot (\rho \boldsymbol{V} v) = \rho g + \nabla \cdot \left(\mu_l \frac{\rho}{\rho_l} \nabla v \right) - \frac{\partial p}{\partial z} - \frac{u_l}{K} \frac{\rho}{\rho_l}(v - v_s) - \frac{C\rho^2}{K^{0.5}\rho_l}|v - v_s|(v - v_s) - \nabla \cdot (\rho f_s f_l \boldsymbol{V}_r v_r) + \nabla \cdot \left(\mu_s v \nabla \left(\frac{\rho}{\rho_l} \right) \right) + \rho g \beta_T (T - T_0) \tag{3}$$

Energy

$$\frac{\partial}{\partial t}(\rho h) + \nabla \cdot (\rho \boldsymbol{V} h) = \nabla \cdot \left(\frac{k}{c_p} \nabla h \right) - \nabla \cdot \left(\frac{k}{c_p} \nabla (h_s - h) \right) - \nabla \cdot (\rho(\boldsymbol{V} - \boldsymbol{V}_s)(h_l - h)) \tag{4}$$

The physical meaning of each term appearing in the above equations can be found in Ref. [13]. In Eqs. (1)–(4), the continuum density, specific heat, thermal conductivity, solid mass fraction, liquid mass fraction, velocity, and enthalpy are defined in Ref. [13].

2.2 Track of Free Surface. The algorithm of volume-of-fluid (VOF) is used to track the dynamic free surface [12]. The fluid configuration is defined by a volume of fluid function, $F(r,z,t)$, which tracks the location of the free surface. The function F takes the value of one for the cell full of fluid and the value of zero for the empty cell. Cells with F values between zero and one are partially filled with fluid and identified as surface cells. The function F is governed by the following equation:

$$\frac{dF}{dt} = \frac{\partial F}{\partial t} + (\boldsymbol{V} \cdot \nabla) F = 0 \tag{5}$$

2.3 Plasma Zone Simulation. Plasma inside the keyhole can be treated as the vapor of the weld material. Although the velocity and pressure change dramatically across the Knudsen layer, the generic translation vapor flow along the keyhole is not significant [14]. Meanwhile, the pressure along the keyhole can be considered to be approximately constant [15]. Since the keyhole is open to the atmosphere, the pressure will be comparable to the atmospheric pressure. Therefore, in the present study, the fluid flow of plasma in the keyhole is neglected and only the temperature field is considered. Since the heat production by viscous dissipation is rather small in laser welding, the energy equation can be simplified as [16]

Table 1 Thermophysical properties of 304 stainless steel and process parameters

Nomenclature	Value
Specific heat of solid phase, c_s (J kg^{-1} K^{-1})	700
Specific heat of liquid phase, c_l (J kg^{-1} K^{-1})	780
Thermal conductivity of solid phase, k_s (W m^{-1} K^{-1})	22
Thermal conductivity of liquid phase, k_l (W m^{-1} K^{-1})	22
Density of solid phase, ρ_s (kg m^{-3})	7200
Density of liquid phase, ρ_l (kg m^{-3})	6900
Dynamic viscosity, μ_l (kg m^{-1} s^{-1})	0.006
Latent heat of fusion, H (J kg^{-1})	2.47×10^5
Solidus temperature, T_s (K)	1670
Liquidus temperature, T_l (K)	1727
Thickness of substrate metal, H_b (mm)	3.0
Radius of substrate metal, R_b (mm)	20.0

$$\frac{\partial}{\partial t}(\rho_{\mathrm{pl}}h_{\mathrm{pl}}) = \nabla\cdot\left(\frac{k_{\mathrm{pl}}}{c_{\mathrm{pl}}}\nabla h_{\mathrm{pl}}\right) + K_{\mathrm{pl}}I_c\exp\left(-\int_0^s K_{\mathrm{pl}}ds\right) + \sum_{m=1}^{n} K_{\mathrm{pl}}I_{r,m}(r,z)\exp\left(-\int_0^{s_m} K_{\mathrm{pl}}ds\right) \quad (6)$$

where h_{pl} and ρ_{pl} represent the enthalpy and density of the plasma, k_{pl} and c_{pl} represent the thermal conductivity and specific heat of the plasma, s is the penetration depth of laser light in the plasma, K_{pl} denotes the inverse Bremsstrahlung (iB) absorption coefficient. When an intense laser pulse interacts with the vapor in the keyhole, a significant amount of laser radiation is absorbed by the ionized particles through iB absorption. For the laser-induced plasma inside the keyhole, the scattering effect is not significant compared with the absorbing and emitting effects. For simplicity, the plasma is assumed to be an absorbing-emitting medium and the laser intensity is exponentially attenuated inside the keyhole plasma.

More details including the assumptions and simplifications about the model and the corresponding boundary conditions can be found in our previous paper [11] and will not be included here.

3 Numerical Method

In computation, the evaluation of the transport equations in the metal and plasma zones is coupled. That is, simulations of the metal and plasma zones provide boundary conditions for each other. However, there are large spatial and physical differences between them. For a compromise between the result convergence and calculation times, different time resolutions were used for these simulations. The governing equations (Eqs. (1)–(6)) and all related supplemental equations and boundary conditions are solved through the following iterative scheme:

1. Equations (1)–(4) are solved iteratively to obtain velocity, pressure, and temperature distributions under the associated boundary conditions for the metal zone.
2. Equation (6) is solved iteratively to obtain the temperature field of the plasma in the keyhole under the associated boundary conditions.
3. Iteration between step (1) and (2).
4. Solve the VOF algorithm Eq. (5) to obtain the new domain for the metal and plasma zones.
5. Update the boundary conditions for the metal and plasma zones.
6. Advance to the next time step until the desired time is reached.

The technique for solving the partial differential equations is given by Wang and Tsai [17]. Following the MAC scheme, the r- and z-velocity components are located at cell face centers on lines of constant r and z respectively, while the pressures, VOF function, temperature, and absorbed laser flux are located at cell centers. Since the temperature and pressure field change more dramatically near the keyhole, a nonuniform grid system with 202 $\times$252 points is used for the total computational domain of 5.0 mm$\times$6.25 mm, in which smaller grids are arranged near the keyhole and larger grids for other parts. Due to the y-axis-symmetry of the domain, only half of the grid points were used in the actual calculation. Due to the large spatial and physical differences between the solid/liquid metal and plasma zones, for a compromise between the result convergence and calculation time, different time resolutions must be used for these simulations. Calculations were executed on the DELL OPTIPLEX GX270 workstations with LINUX-REDHAT 9.0 OS and took 6 h of CPU time

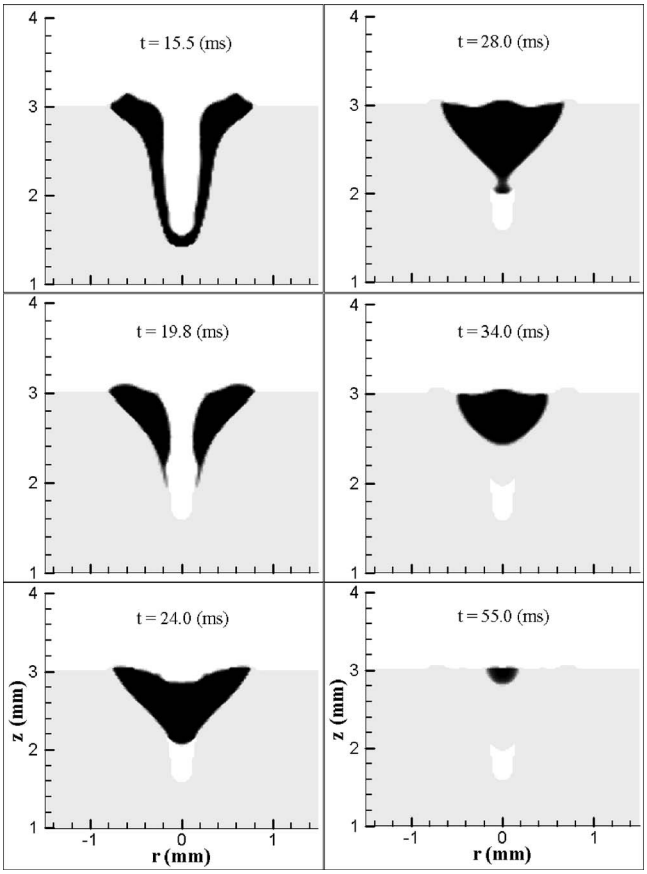

Fig. 2 A sequence of liquid metal evolution showing porosity formation

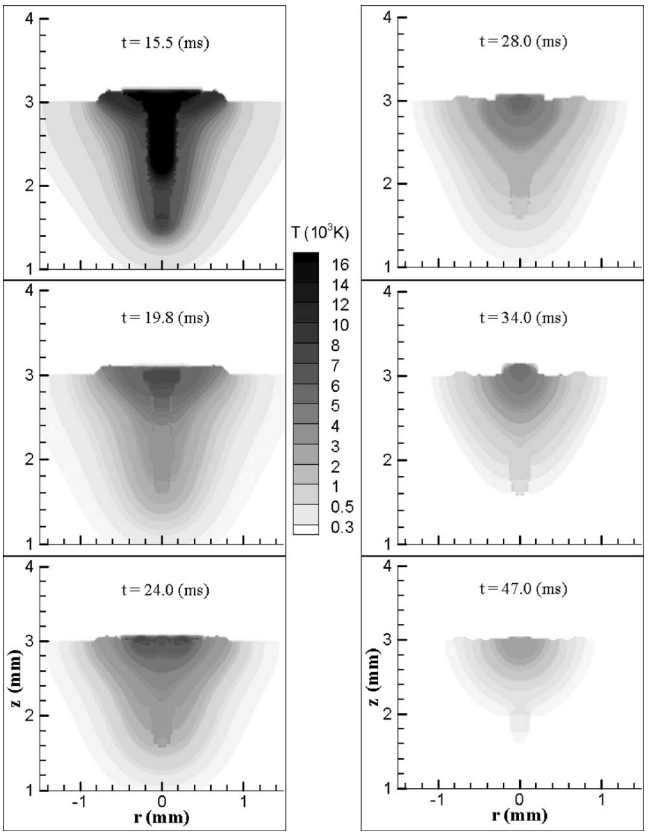

Fig. 3 The corresponding temperature distributions for the case as shown in Fig. 2

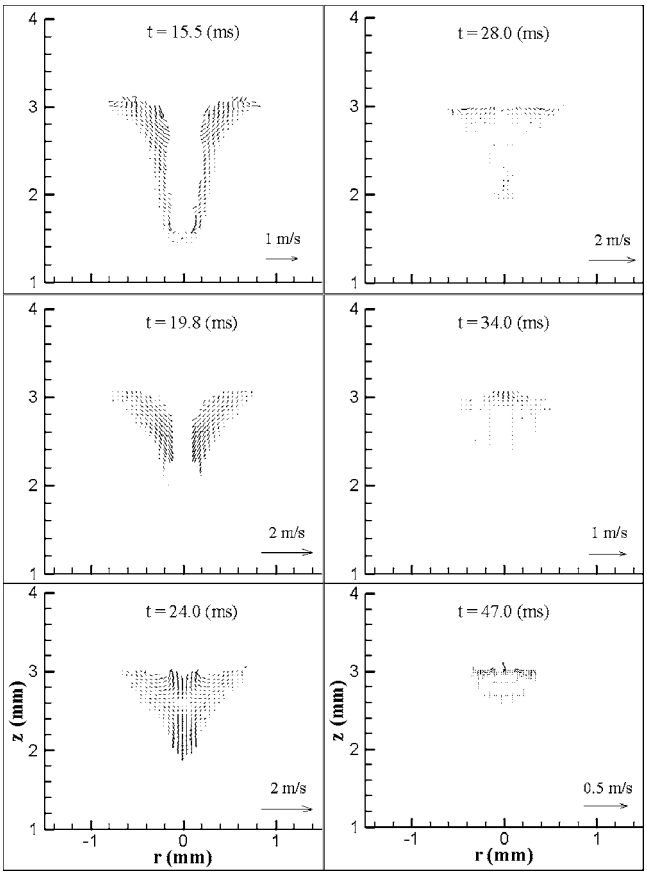

Fig. 4 The corresponding velocity distributions for the case as shown in Fig. 2

to simulate about 100 ms of real-time welding. The average time step is 10^{-4} s and the smallest time step is about 10^{-6} s.

4 Results and Discussion

The thermophysical properties and welding conditions used in the present study are summarized in Table 1. The following welding conditions are assumed in the model: the radius of the laser beam at focus is 0.25 mm, the laser beam energy is a Gaussian distribution, and the laser beam energy and pulse shape vary according to different study cases. The divergence of the laser beam is assumed to be negligible for a 3.0 mm metal thickness.

4.1 Porosity Formation. Since the keyhole formation process has been discussed before [11], the following discussions will be focused on the keyhole collapse process. Figure 2 shows a typical keyhole collapse and solidification process in pulsed laser welding with laser power at 1.7 kW and pulse duration time at 15.0 ms. The corresponding temperature and velocity evolutions are given in Figs. 3 and 4, respectively.

As shown in Fig. 2, once the laser is shut off at $t=15.0$ ms, the hot plasma is the only heat input source to irradiate the keyhole wall. Since the heat capacity of the plasma is very small, the temperature of the plasma drops very quickly after the laser is turned off, as shown at $t=15.5$ ms in Fig. 3. At $t=19.8$ ms, the keyhole plasma almost completely disappears. Furthermore, due to the large aspect ratio of the keyhole and the high temperature gradient, the heat loss conducted from the hot keyhole wall to the surrounding metal is very strong. Hence, as shown in Fig. 3, the temperature of the keyhole wall drops very quickly, especially for the lower part of the keyhole having only a thin layer of the liquid metal. Due to this quick temperature drop, the thin layer of liquid metal on the bottom of the keyhole solidifies very quickly after the shut-off of the laser power, as shown at $t=19.8$ ms in Fig. 2.

As shown in Fig. 3, after the laser beam is shut off, the temperature on the bottom surface of the keyhole drops faster than that on the upper surface, so the temperature gradient along the

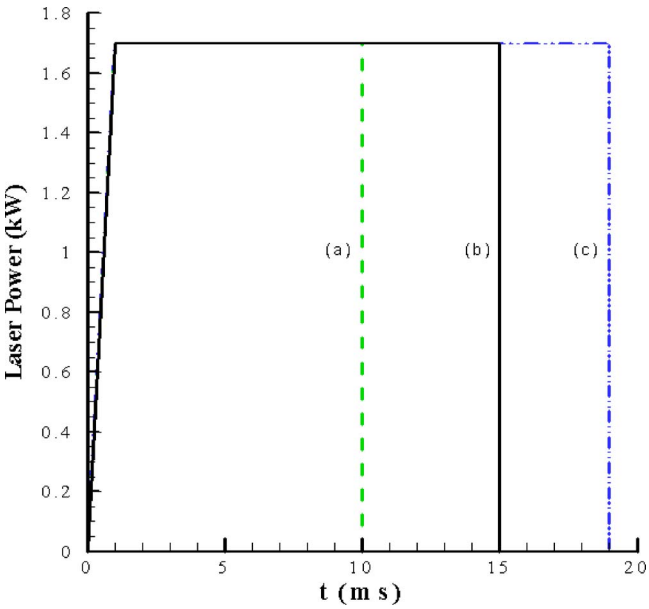

Fig. 5 Laser pulse profile used to generate (*a*) a small depth-to-width ratio keyhole; (*b*) a medium depth-to-width ratio keyhole; and (*c*) a large depth-to-width ratio keyhole

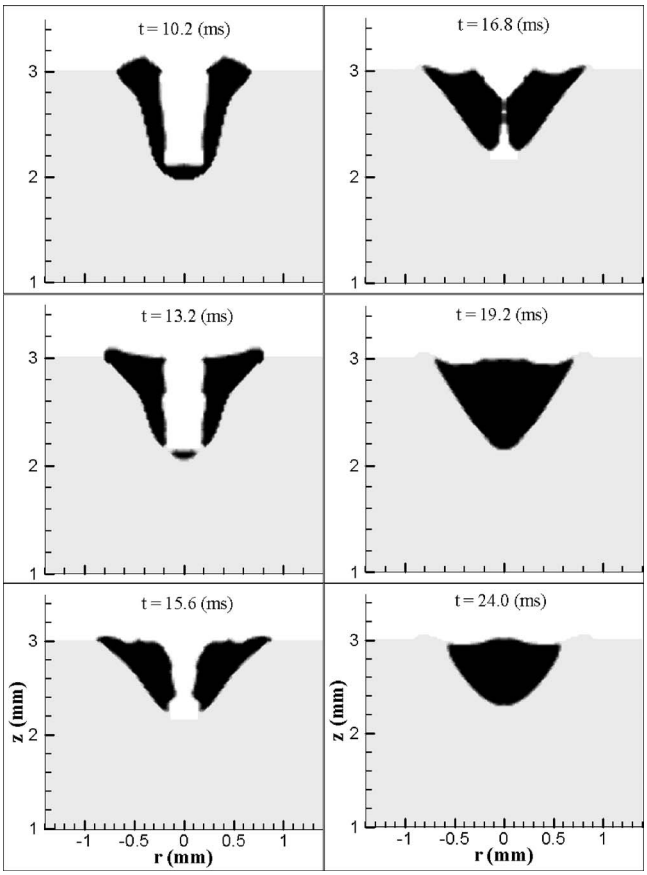

Fig. 6 A sequence of liquid metal evolution during the keyhole collapse and solidification in a small depth-to-width ratio keyhole welding process

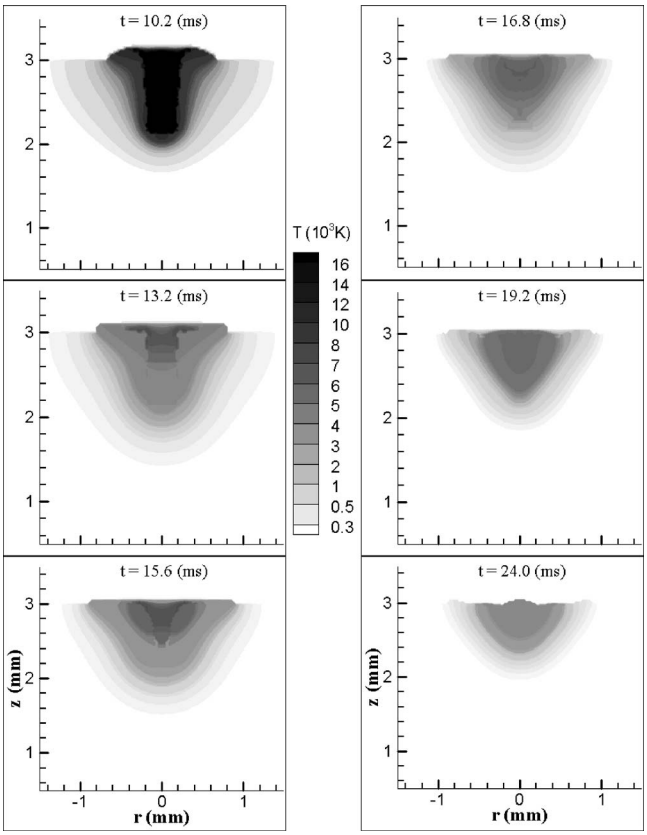

Fig. 7 The corresponding temperature distributions for the case as shown in Fig. 6

keyhole wall decreases. This causes the temperature-dependent Marangoni shear stress to decrease accordingly. Meanwhile, with the removal of the recoil pressure due to the shut-off of the laser, the recoil pressure-driving hydrodynamic pressure of the squeezed liquid metal also decreases very quickly. Consequently, surface tension and hydrostatic pressure become dominant and drive the liquid metal to have a tendency to fill back the keyhole. As shown in Fig. 4 at $t=15.5$ ms, the liquid metal located on the upper part of the keyhole starts to flow inward and downward under the hydrostatic pressure and surface tension. Since the liquid metal layer is thicker on the top and the flow friction along the liquid-solid interface is larger for a thinner liquid layer, the backfilling velocity for the liquid metal on the upper part is accelerated more quickly than those on the lower part of the keyhole. As shown in Fig. 2, the keyhole is closed on the top first. After the keyhole is closed on the top, the liquid metal continues to flow downward along the keyhole wall. When the liquid metal flows downward along the solidified keyhole wall, its velocity is decreased by the friction force of the cool keyhole wall. Meanwhile the solid-liquid interface moves inward to the centerline of the keyhole because of the strong heat conduction loss to the surrounding metal along the keyhole wall. As shown in Fig. 2 from $t=24.0$ ms to $t=28.0$ ms, the liquid region shrinks as the liquid refills the keyhole, especially for the liquid metal at the bottom because of higher conduction heat loss and lower heat capacity there. Finally the bottom of the downward flowing liquid metal completely solidified before it can reach the bottom of the keyhole as shown at $t=28.0$ ms. From then on, although there is still a certain amount of liquid metal on the top, this part of liquid metal cannot continue to flow downward, which leaves a pore or void at the root of the keyhole.

4.2 Aspect Ratio of Keyhole Versus Size of the Pore. The aspect ratio is the ratio of keyhole depth to its width. In laser welding, especially in keyhole mode laser welding, the aspect ratio can be very large, which is one of the main advantages of laser welding. However, porosity is frequently found in a deep keyhole laser weld. The following studies are addressed toward investigating the effect of keyhole aspect ratio on porosity formation. In the studies, the laser power and keyhole width are fixed and the keyhole depth is determined by the laser pulse duration. By changing the pulse duration of the laser beam, different aspect ratio keyholes can be obtained in different study cases. In the following discussions, small aspect ratio means the ratio is less than 0.6, while the medium aspect ratio means the ratio is larger than 0.6 and less than 1.0. If the ratio is larger than 1.5, it is considered as a large aspect ratio.

4.2.1 Small Aspect Ratio Keyhole. The laser power used in this study was 1.7 kW and the radius of the laser beam at the focus was 0.2 mm. As shown in Fig. 5(*a*), the laser power was set at 1.7 kW within 1.0 ms and was turned off at $t=10.0$ ms. Figure 6 shows the keyhole collapse and solidification processes. The corresponding temperature and velocity distributions are given, respectively, in Figs. 7 and 8.

As shown in Fig. 6 at $t=10.2$ ms, alot of liquid metal was squeezed from the bottom of the keyhole to its shoulder by the laser-induced recoil pressure during the keyhole formation process. After the laser beam was turned off at $t=10.0$ ms, the laser-induced recoil pressure very quickly disappeared. Hence, there was no strong driving force to push the liquid metal to flow toward the top of the keyhole. Meanwhile, as shown in Fig. 7 from $t=10.2$ ms to $t=13.2$ ms, the temperature of the keyhole plasma and liquid metal very quickly drops due to the shut-off of the laser power. Once the liquid metal temperature drops below 2150 K, the surface tension gradient coefficient $\partial\gamma/\partial T$ will turn positive.

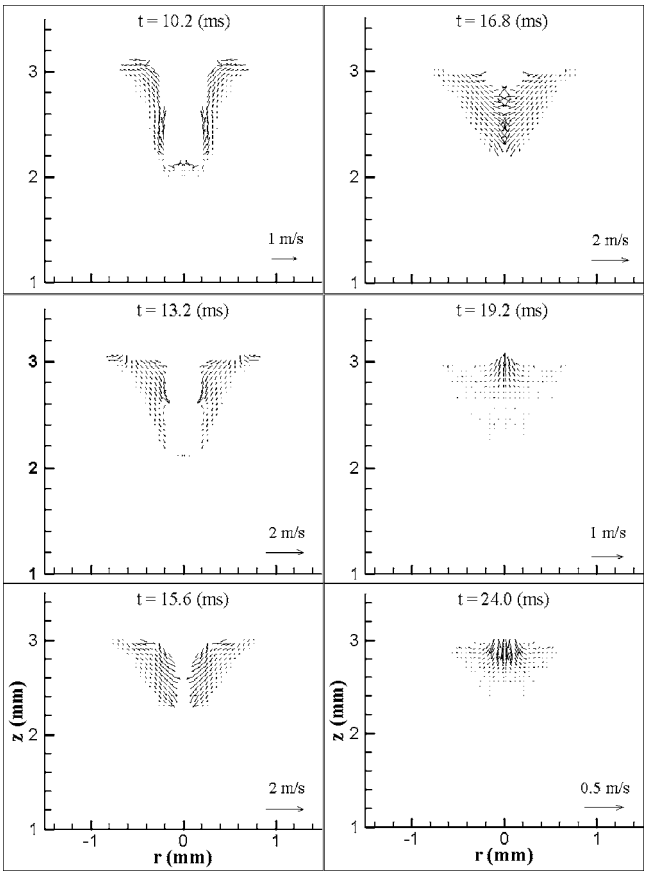

Fig. 8 The corresponding velocity distributions for the case as shown in Fig. 6

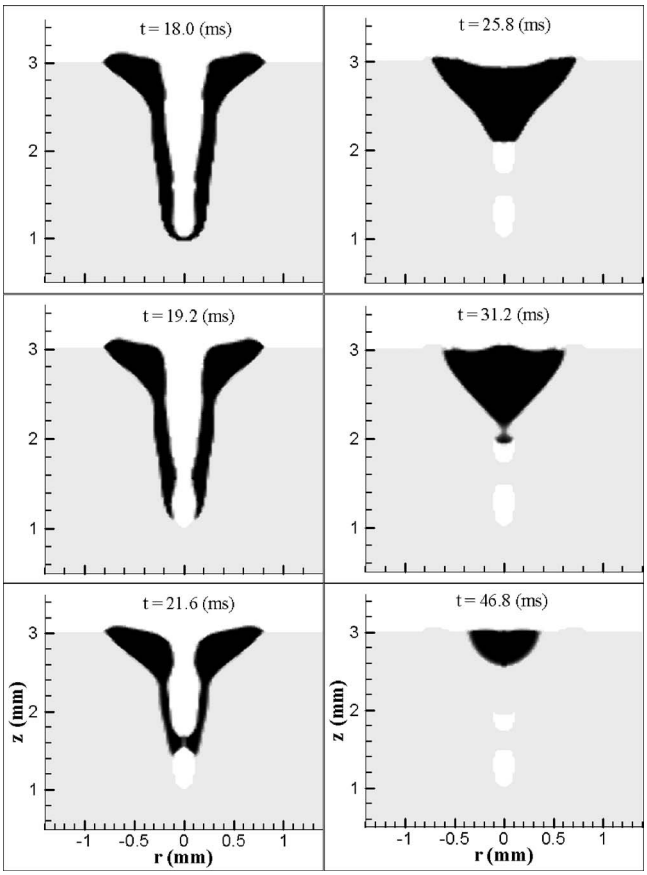

Fig. 9 A sequence of liquid metal evolution during the keyhole collapse and solidification in a large depth-to-width ratio keyhole welding process

Since at this time the temperature gradient from the center to the shoulder is still positive, it will cause the temperature-dependent surface tension force to change its direction to negative along the weld pool surface. This will drive the liquid metal to flow inward. This surface tension force combined with the hydrostatic pressure will drive the accumulated liquid metal on the top to have a tendency to fill back the keyhole. As shown in Fig. 6 at $t=13.2$ ms, the keyhole starts to collapse from the top under these forces. Since it takes time for the liquid metal flow to change its direction, the liquid metal is still flowing outward and upward at $t=10.2$ ms in Fig. 8. With the continuous acceleration of the surface tension force and hydrostatic pressure, the liquid metal finally flows downward and inward at $t=13.2$ ms.

In Fig. 6 at $t=10.2$ ms, after the shut-off of the laser, since there is no heat input, the solidification process quickly becomes dominant. Comparing the figures at $t=10.2$ ms, $t=13.2$ ms, and $t=15.6$ ms in Fig. 6, it is easy to find the liquid metal on the bottom of the keyhole almost completely solidifies at $t=15.6$ ms due to the solidification process. As indicated by previous discussions of the porosity formation process, it is known that porosity formation is determined by two competing processes: the backfilling process and the solidification process. Since the keyhole depth is small in this case, it requires shorter time for the liquid metal on the top to fill back the bottom of the keyhole. As shown in Fig. 6, although the liquid metal on the bottom of the keyhole almost completely solidifies at $t=15.6$ ms, since the keyhole is shallow, the liquid metal flowing downward from the top can still reach the keyhole bottom at $t=19.2$ ms and fill up the keyhole before complete solidification. Hence, no porosity is found in the final weld in this case.

4.2.2 Medium Aspect Ratio Keyhole. The laser power density and the radius of the laser beam at the focus are kept the same as those in the previous case to ensure the same width of the keyhole. As shown in Fig. 5(*b*), the laser beam is held for a longer time to 15.0 ms to get a deeper keyhole. The keyhole collapse process after shut-off of the laser power is shown in Fig. 2. The corresponding temperature and velocity distributions are given, respectively, in Figs. 3 and 4. As discussed in the previous porosity formation section, a pore/void is found at the root of the keyhole in this case since the solidification process exceeds the backfilling process.

4.2.3 Large Aspect Ratio Keyhole. In this case, the laser power and the radius of the laser beam are still kept the same as those in the previous two cases to ensure the same keyhole width. As shown in Fig. 5(*c*), the laser beam is held for a longer time to 19.0 ms to produce an even deeper keyhole. Figure 9 shows the keyhole collapse and solidification processes. The corresponding temperature and velocity distributions are given, respectively, in Fig. 10 and 11. As shown in Fig. 9 at $t=18.0$ ms, since the keyhole is deeper, only a small amount of laser beam energy can reach the bottom of the keyhole and there is only a very thin layer of liquid metal on the bottom of the keyhole. After the shutoff of the laser beam, due to less heat capacity and strong heat loss on the bottom of the keyhole, the thin layer of liquid metal on the bottom of the keyhole quickly solidifies at $t=19.2$ ms. Meanwhile, with the actions of hydrostatic pressure and surface tension force, the liquid metal in the upper and middle part of the keyhole is flowing downward along the keyhole wall. While flowing along the solidified keyhole wall, since there is not too much liquid metal there and its heat capacity is small, the downward flowing liquid metal quickly cools down and its downward velocity rap-

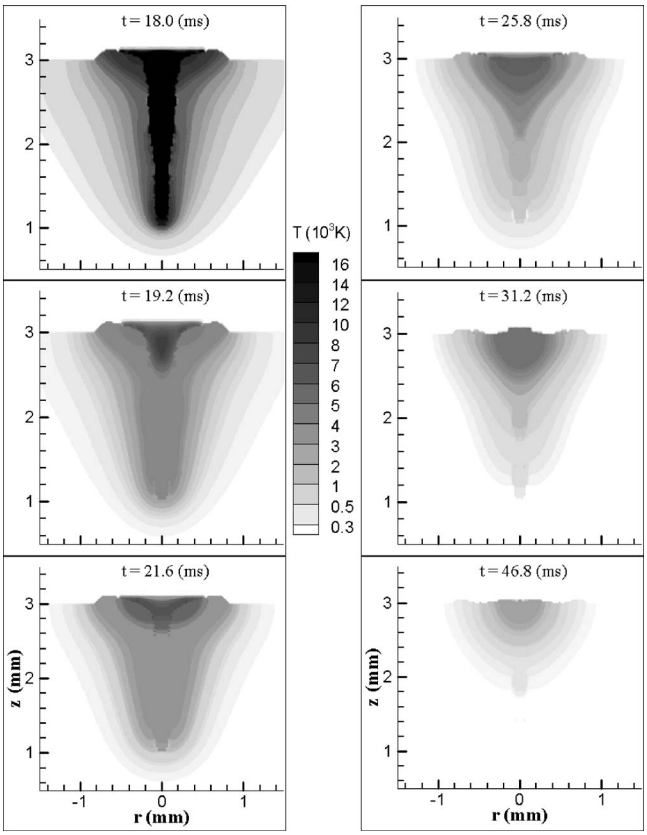

Fig. 10 The corresponding temperature distributions for the case as shown in Fig. 9

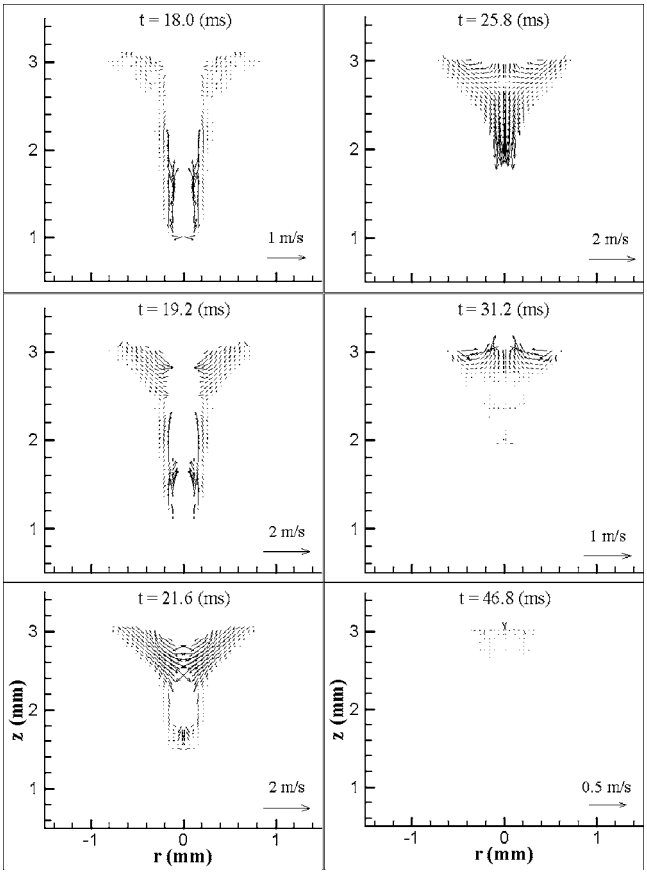

Fig. 11 The corresponding velocity distributions for the case as shown in Fig. 9

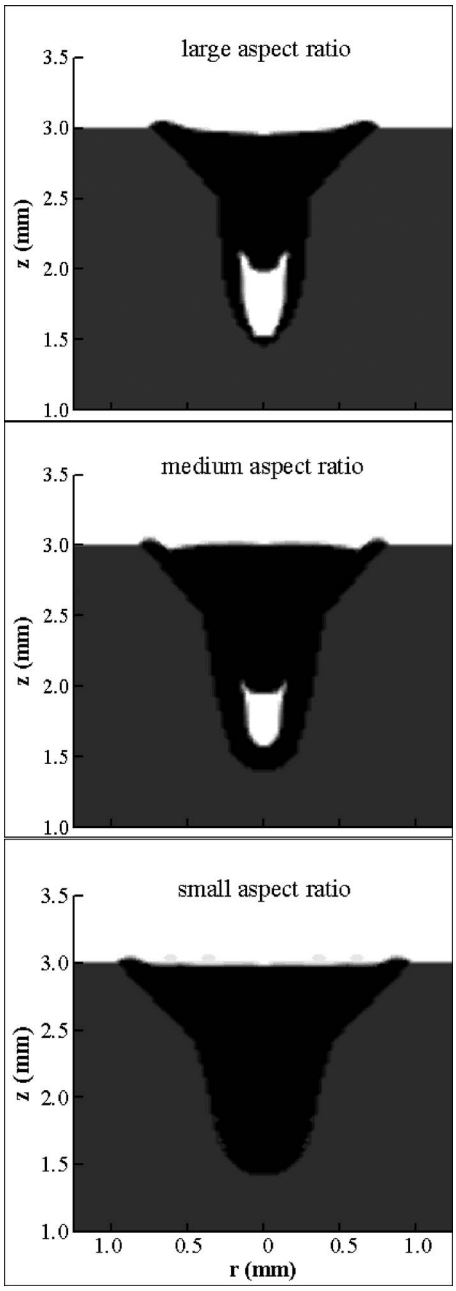

Fig. 12 The effect of depth-to-width ratio on pore formation for constant keyhole depth

idly decreases due to the friction force of the cool keyhole wall. After a very short period of time, when the downward flowing liquid metal reaches a certain depth ($z=1.5$ mm in Fig. 9), the bottom velocity of this downward flowing liquid metal decreases to almost zero and its bottom completely solidifies. Although, at this time, there is still some liquid metal on the top ($z>1.5$ mm in Fig. 9), this amount of liquid metal is blocked by the solidified metal and cannot flow downward any farther. At $t=25.8$ ms, this small amount of liquid metal completely solidifies in the middle of the keyhole. So, a pore/void is formed at the root of the keyhole.

Meanwhile, with the combined actions of surface tension force and hydrostatic pressure, the liquid metal on the top of the keyhole is still flowing downward and inward to fill back the keyhole. It takes a while for the liquid metal in the middle of the keyhole wall to change its flow direction as shown in Fig. 11, when t

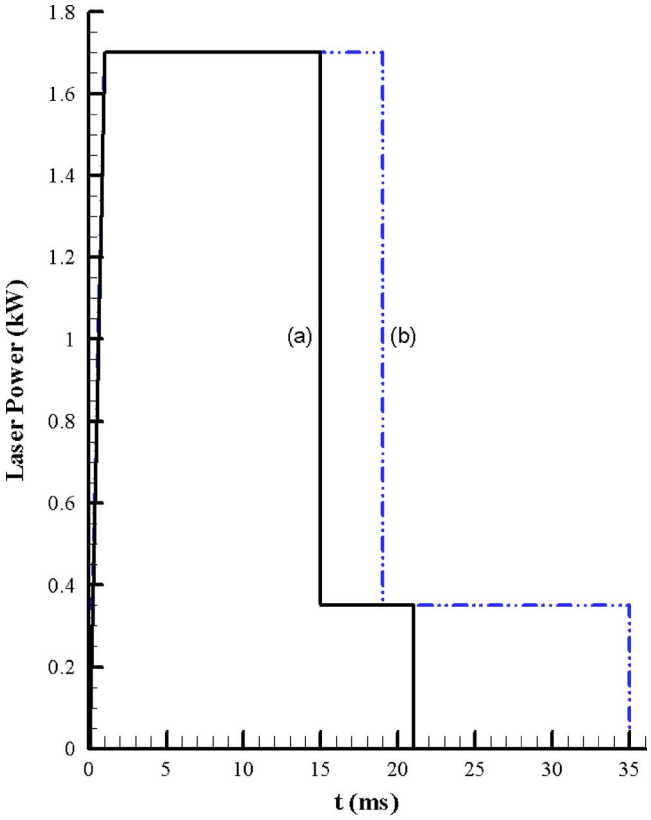

Fig. 13 Laser pulse profiles used to reduce/eliminate pore/void formation for a keyhole with (*a*) a medium depth-to-width ratio and (*b*) a large depth-to-width ratio

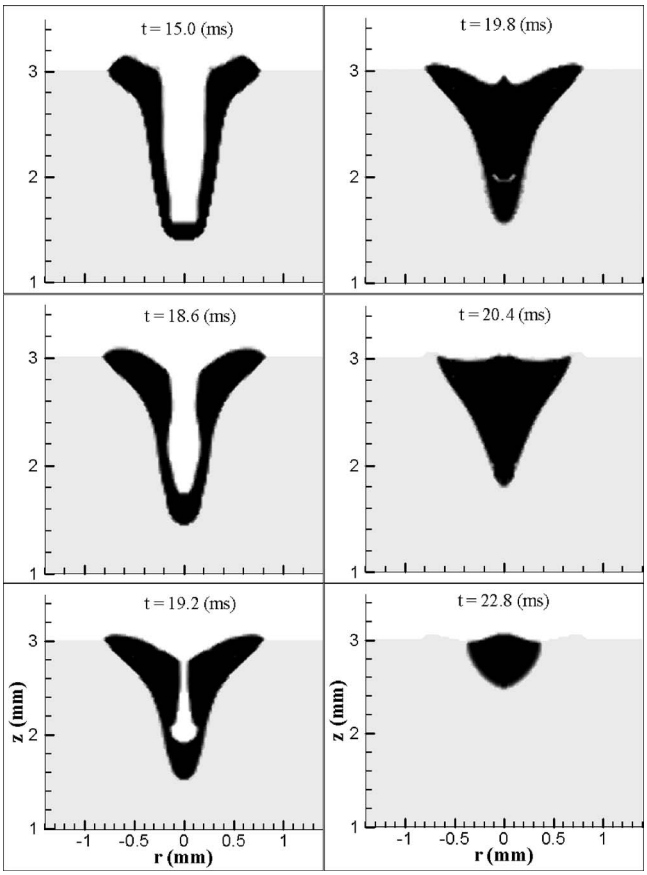

Fig. 14 A sequence of liquid metal evolution during pore/void reduction/elimination for a medium depth-to-width ratio keyhole welding process by using the pulse profile in Fig. 13(*a*)

>21.6 ms, the liquid metal changes its direction to flow downward. The magnitude of the velocity is relatively small and the amount of liquid metal in the middle of the keyhole wall is small, so the solidification process becomes dominant. Compared to that at $t=19.2$ ms, the liquid metal region in the middle part of the keyhole shrinks at $t=21.6$ ms due to the solidification process. At $t=25.8$ ms, the keyhole is closed from the top and the downward flowing liquid metal very quickly cooled down. The whole liquid region shrinks from outside to inside and from bottom to top and its velocity is decreased by the friction forces. At $t=31.2$ ms, when the downward flowing liquid metal reaches the middle of the keyhole (at $z=2.0$ mm in Fig. 9), the bottom part almost completely solidifies. Hence, the remaining liquid metal on the top cannot flow downward farther. Another pore/void was formed in the middle of the keyhole in the final weld. In the previous three case studies, the keyhole width was fixed and the change of the aspect ratio was controlled by changing the keyhole depth. It was found that for a small depth-to-width keyhole, there was no porosity found in the final weld. For a medium and large depth-to-width aspect ratio keyhole, porosity was found and for a large aspect ratio keyhole, the porosity size was larger. In the following, the porosity formation process was further studied using a fixed keyhole depth and varying keyhole width conditions. Results are shown in Fig. 12 and similar phenomena are found. For a small depth-to-width aspect ratio keyhole, there was no porosity found in the final weld bead. For a medium and large aspect ratio keyhole, porosity was found. This can also be explained through investigation of the porosity formation process. As the keyhole width increases, the backfilling time (the time from laser light removal to when the liquid metal stops filling back) will correspondingly increase due to the increasing amount of liquid metal on the top and decreasing solidification rate. This gives more time for the liquid metal to flow downward to fill the keyhole. Moreover, larger keyhole diameter leads to a smaller wall friction, which also increases backfilling speed of the liquid metal. Both factors help to reduce porosity formation in the final welds.

4.3 Porosity Prevention/Elimination by Laser Pulse Control. From the aforementioned studies, it is clear that if the downward flowing liquid metal can fill up the bottom of the keyhole before complete solidification, there will be no porosity in the final weld. This can be achieved in two ways: (1) delaying the solidification process to increase the backfilling time; (2) increasing the backfilling speed of the liquid metal. The following studies will be focused on studying the effectiveness of the first method for delaying the solidification process. This can be realized by controlling the laser pulse shape and power density.

4.3.1 Medium Aspect Ratio Keyhole. As inspired by the previous studies, at $t=15.0$ ms if the laser is not completely shut off, but reduced to a moderate power level, whose density is not large enough to produce a recoil pressure, but large enough to provide additional heat for the weld pool. Then the solidification process will be delayed by this additional heat input and, consequently, the backfilling time will be increased. This increased backfilling time can allow the downward flowing liquid metal to fill up the keyhole. As shown in Fig. 13(*a*) at $t=15.0$ ms, the laser power is reduced to 0.35 kW, one-fifth of its peak value, and lasts for another 6.0 ms. This reduced laser power is small enough to prevent the recoil pressure effect on the keyhole wall while it can provide enough heat to delay the solidification process. Figure 14 shows the keyhole collapse and solidification processes. The corresponding temperature and velocity evolutions are shown in Figs. 15 and 16.

As shown in Fig. 14, with the removal of the main laser power

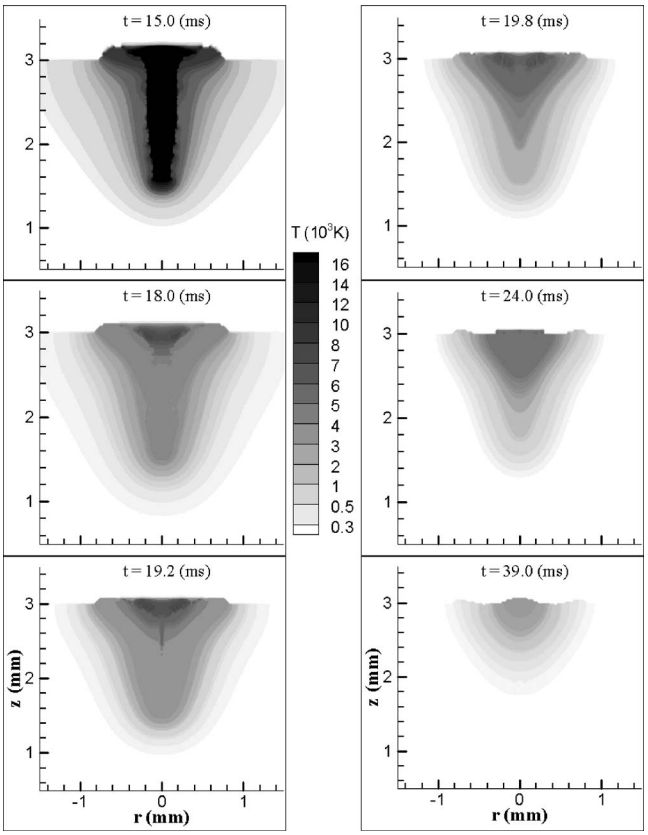

Fig. 15 The corresponding temperature distributions for the case as shown in Fig. 14

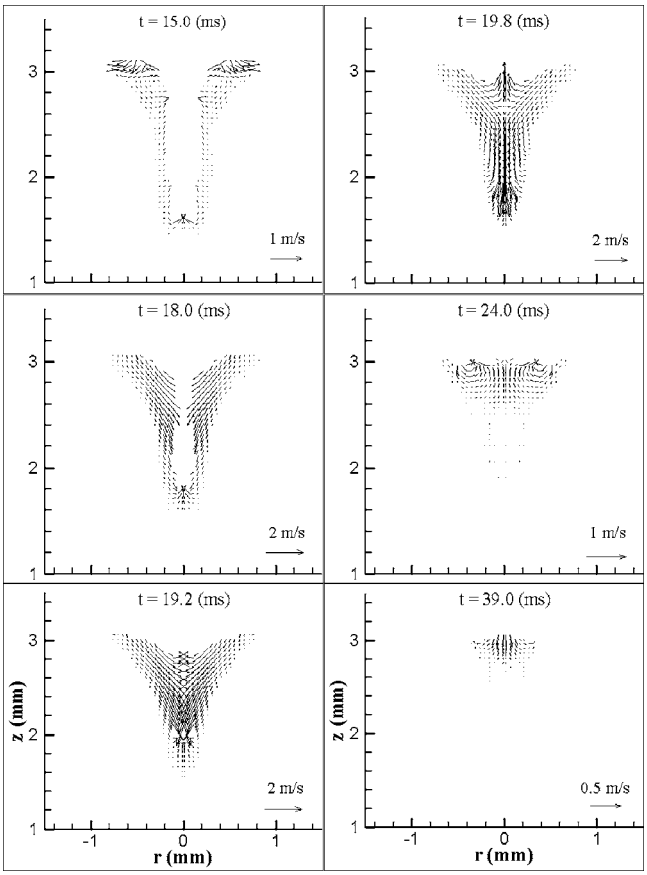

Fig. 16 The corresponding velocity distributions for the case as shown in Fig. 14

at $t=15.0$ ms, the keyhole begins to collapse. Meanwhile the reduced laser power continues to heat the keyhole surface, which allows liquid metal at the bottom of the keyhole to remain liquid at $t=18.6$ ms as compared to what occurred in Fig. 2. As the liquid metal from the shoulder of the keyhole approaches the center, it prevents part of the laser light from reaching the bottom surface of the keyhole. This will lead to a temperature decrease on this part of the keyhole wall. However, the multiple reflections on the keyhole wall will reflect some laser energy to the keyhole wall where laser light cannot radiate directly. This helps to delay the solidification process along the keyhole wall. At $t=19.2$ ms, the keyhole is almost completely closed from the top and from then on only a very small portion of the laser light can reach the bottom of the keyhole. However, as shown in Fig. 15, the temperature on the bottom of the keyhole wall is still hot enough to allow the metal to stay liquid. At this time, most of the laser energy is used to heat the liquid metal on the top, which can help the liquid metal on the top to flow downward. As shown in Fig. 16 at $t=19.2$ ms, the downward momentum of the liquid metal is strong. Hence, within a short period of time, the downward flowing liquid metal almost completely fills up the keyhole at $t=19.8$ ms and the porosity which was found in Fig. 2 has been eliminated. Although some gas is enclosed, the gas is surrounded by liquid metal, which can continue to flow into the gas region. During the backfilling process, the hydrostatic pressure continues to accelerate the melt flow, which facilitates the backfilling process. The downward flowing liquid metal makes the gas region smaller and smaller. In addition, since the gas is a mixture of shielding gas and metal vapor, some of it will be dissolved in the liquid metal during the compression process and eventually the gas region will completely disappear in the metal liquid, as shown at $t=20.4$ ms in Fig. 14. This result is consistent with the experimental observations by Katayama and Matsunawa [3].

4.3.2 Large Aspect Ratio Keyhole. As shown above, through providing additional heat to increase the backfilling time, controlling the laser pulse shape is a very effective way to eliminate porosity formation for a medium aspect ratio keyhole laser weld. In the following study, the effectiveness of this method is investigated for a large aspect ratio keyhole. As shown in Fig. 13(*b*) at $t=19.0$ ms, the laser power density is reduced to 0.35 kW. Since the keyhole is deeper, this reduced laser power is held for a longer time (35.0 ms) to provide more additional heat. Figure 17 shows the keyhole collapse and solidification processes and the corresponding temperature and velocity distributions are shown in Figs. 18 and 19, respectively.

As shown in Fig. 18, due to the additional heat input after the removal of the main laser power, the plasma temperature drops slower from $t=18.0$ ms to $t=19.2$ ms as compared to that in Fig. 10. This is helpful to keep the liquid metal on the bottom of the keyhole and to delay the solidification process of the liquid metal on the side of the keyhole. This is clearly indicated at $t=19.2$ ms in Fig. 17, due to irradiation from the hot plasma and the additional heat input from the laser, the metal on the keyhole bottom is still a liquid and the amount of the liquid metal on the side of the keyhole is almost the same as that at $t=18.0$ ms.

However, since the keyhole aspect ratio is larger in this case, more liquid metal is located on the shoulder, which leaves a larger crater on the top of the keyhole. Meanwhile, the reduced laser energy can keep the temperature of the liquid metal on the top high, which facilitates the melt flow there. Hence, at $t=19.0$ ms, after the removal of the main laser power, with the action of surface tension force and hydrostatic pressure, this large crater will drive the hot liquid metal on the top to move inward easily to close the keyhole and shorten the time for keyhole closure. When the liquid metal from the shoulder of the keyhole approaches the

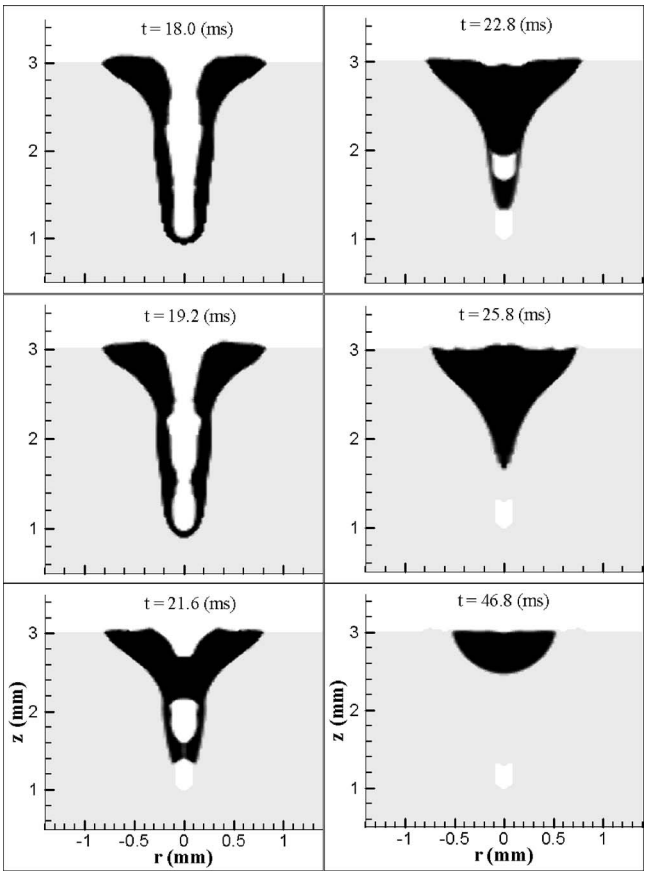

Fig. 17 A sequence of liquid metal evolution during pore reducing/elimination for a large depth-to-width ratio keyhole welding process by using the pulse profile in Fig. 13(*b*)

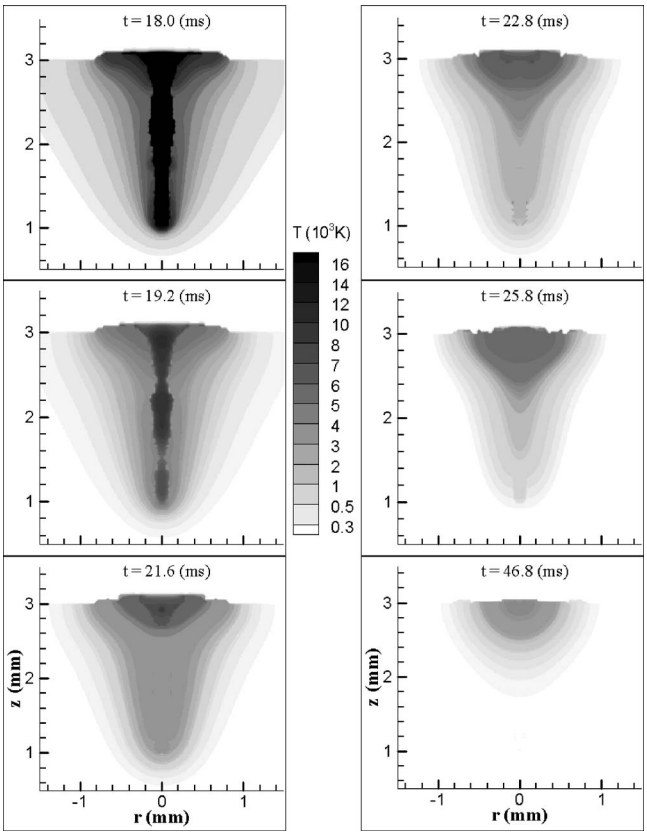

Fig. 18 The corresponding temperature distributions for the case as shown in Fig. 17

keyhole center, the amount of the laser beam energy entering the keyhole becomes smaller and smaller. Although the multiple reflections can still bring some laser light to heat the keyhole wall where the laser light cannot radiate directly, the total area is relatively large compared with that in a medium aspect ratio keyhole, the heat input per unit area is reduced for a high aspect ratio keyhole. This facilitates the solidification process on the keyhole wall and bottom. As shown in Fig. 18, at $t=19.2$ ms, the temperature of the liquid on the bottom quickly decreases due to the heat loss to the surrounding metal and the reduced incoming heat input caused by the keyhole collapse from the top. At $t=21.6$ ms in Fig. 17, the keyhole is completely closed on the top, then laser light cannot enter the keyhole and the liquid metal on the bottom of the keyhole quickly solidifies. Although, with the action of hydrostatic pressure, the liquid metal on the upper and middle part of the keyhole flows downward to fill the keyhole, due to the fast solidification rate, at $t=22.8$ ms the bottom part of the downward flowing liquid metal completely solidifies at $z=1.65$ mm in Fig. 17. After that, no liquid metal can reach the bottom of the keyhole and a pore/void shown in Fig. 9 is still found at the root of the keyhole.

However, there is no pore or void found in the upper part of the keyhole in this case, which is different from that shown in Fig. 9. This is easy to understand. As shown in Fig. 17 at $t=21.6$ ms, the keyhole is fully closed on the top. From then on, although the laser light cannot penetrate into the keyhole any more, it still can heat the liquid metal on the top and keep the temperature of the liquid metal high, which facilitates the liquid metal to flow downward against small friction force. Although, at this time, part of the liquid metal solidifies along the keyhole wall due to the solidification process. Since there is a considerable amount of liquid metal with high temperature on the top as shown in Fig. 18 and the downward momentum of the liquid metal is strong as shown in Fig. 19, this hot downward flowing liquid metal can eventually reach the top of the previously solidified metal (at $z=1.4$ mm) and fill up the keyhole there at $t=25.8$ ms. Hence, the pore/void shown in the middle part of the keyhole in Fig. 9 has been eliminated.

5 Conclusions

Porosity formation is investigated in a keyhole mode laser welding process using mathematical models. The influence of depth-to-width aspect ratio of the keyhole on porosity formation is discussed. Based on these investigations, the prevention/elimination of porosity through laser pulse control is put forward. The conclusions obtained are listed as follows.

Porosity is formed during the keyhole collapse and solidification process. The formation of porosity has a close relationship with two competing factors: (1) the solidification rate of the liquid metal, and (2) the backfilling speed of the liquid metal. If the backfilling speed of the liquid metal is not large enough to make the downward flowing liquid metal completely fill up the keyhole before its complete solidification, a pore/void will be found in the final weld. Aspect ratio of the keyhole has major influence on porosity formation. For a small depth-to-width aspect ratio keyhole welding process, there is no pore/void found in the final weld. For a medium or large aspect ratio keyhole welding process, porosity is found in the final weld. The larger the aspect ratio, the easier the porosity is formed and the larger the size of the pore/void.

The mechanism of preventing porosity formation through laser pulse shape control is to delay the solidification process, which allows the liquid metal in the weld pool to have enough time to flow downward to fill up the keyhole. This method is very effec-

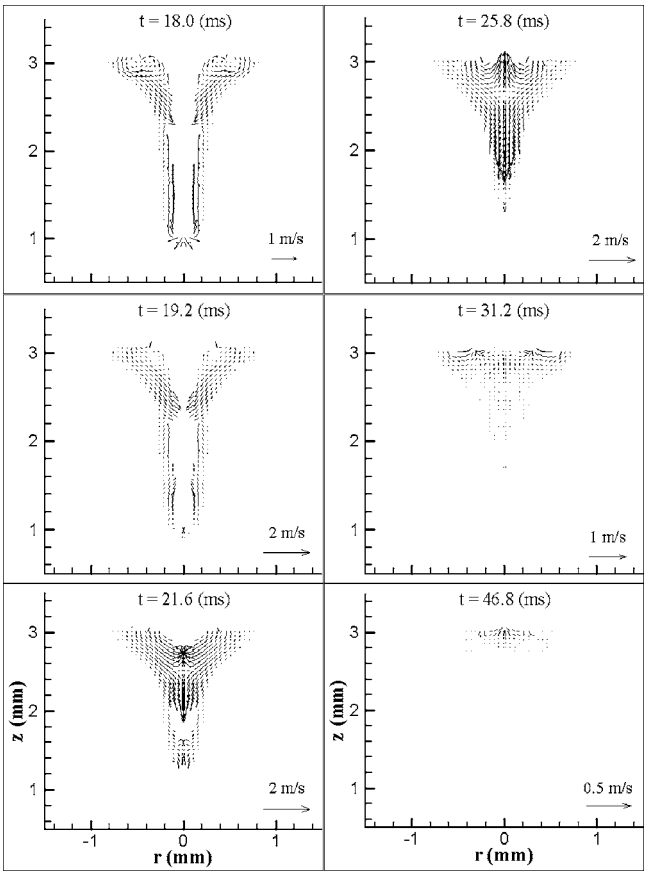

Fig. 19 The corresponding velocity distributions for the case as shown in Fig. 17

tive in eliminating porosity formation for a medium aspect ratio keyhole. But for a large aspect ratio keyhole, it has its limitations. The pore/void in the middle of the keyhole can be eliminated, but it cannot eliminate porosity formation at the root of the keyhole. Other porosity prevention methods, such as increasing the backfilling speed of the liquid metal via application of electromagnetic force to eliminate the porosity in large aspect ratio keyhole laser welding will be investigated in future studies.

Acknowledgment

It is gratefully acknowledged that this research is partially supported by the General Motors Corporation. Also, special thanks go to Professor Terry F. Lehnhoff for his guidance in writing and for beneficial discussions with him.

Nomenclature

c_p = specific heat for metal
c_{pl} = specific heat for keyhole plasma
C = coefficient defined in Eq. (2)
f = mass fraction
F = volume of fluid function
g = gravitational acceleration
h = enthalpy for metal
h_{pl} = enthalpy for plasma
H_b = thickness of base metal
I = laser beam intensity
k = thermal conductivity for metal
K = permeability function defined in Eqs. (2) and (3)
K_{pl} = plasma laser absorption coefficient
p = pressure for metal zone simulation
r-z = cylindrical coordinate system
R_b = radius of base metal
s = penetration depth of laser light in plasma
t = time
T = temperature
u = velocity in the r-direction
v = velocity in the z-direction
$\boldsymbol{V}$ = velocity vector

Greek symbols

β_T = thermal expansion coefficient
μ = dynamic viscosity
ρ = density for metal

Subscripts

0 = initial value
c = original incident laser light
l = liquid phase
r = relative to solid velocity
(r,m) = mth reflected laser beam
pl = plasma
s = solid phase

References

[1] Ishide, T., Tsubota, S., Nayama, M., Shimokusu, Y., Nagashima, T., and Okimura, K., 1999, "10 kW Class YAG Laser Application for Heavy Components," *SPIE High-Power Lasers in Manufacturing*, Osaka, Vol. 3888, pp. 543–550.
[2] Katayama, S., Seto, N., Kim, J., and Matsunawa, A., 1997, "Formation Mechanism and Reduction Method of Porosity in Laser Welding of Stainless Steel," in *Proceedings of ICALEO*, Sec. G, pp. 83–92.
[3] Katayama, S., and Matsunawa, A., 1998, "Formation Mechanism and Prevention of Defects in Laser Welding of Aluminum Alloys," in *Proceedings of CISFFEL 6*, Vol. 1, pp. 215–222.
[4] Katayama, S., Seto, N., Kim, J., and Matsunawa, A., 1998, "Formation Mechanism and Suppression Procedure of Porosity in High Power Laser Welding of Aluminum Alloys," in *Proceedings of ICALEO*, Sec. C, pp. 24–33.
[5] Katayama, S., Seto, N., Mizutani, M., and Matsunawa, A., 2000, "Formation Mechanism of Porosity in High Power YAG Laser Welding," in *Proceedings of ICALEO*, Sec. C, pp. 16–25.
[6] Seto, N., Katayama, S., and Matsunawa, A., 1999, "A High – Speed Simultaneous Observation of Plasma and Keyhole Behavior during High Power CO_2 Laser Welding," in *Proceedings of ICALEO*, Sec. E, pp. 17–19.
[7] Katayama, S., Kohsaka, S., Mizutani, M., Nishizawa, K., and Matsunawa, A., 1993, "Pulse Shape Optimization for Defect Prevention in Pulsed Laser Welding of Stainless Steels," in *Proceedings of ICALEO*, pp. 487–497.
[8] Katayama, S., Kobayashi, Y., Seto, N., Mizutani, M., and Matsunawa, A., 2000, "Effect of Vacuum on Penetration and Defects in Laser Welding," in *Proceedings of ICALEO*, Sec. C, pp. 182–191.
[9] Tsukamoto, S., Kawaguchi, I., and Arakane, G., 2000, "Suppression of Welding Defects in Deep Penetration CO2 Laser Welding," in *Proceedings of ICALEO*, Sec. C, pp. 7–15.
[10] Todate, A., Ueno, Y., Katsuki, M., Katayama, S., and Matsunawa, A., 2000, "YAG Laser Weldability of Carbon Steel in CO_2 Shielding Gas," in *Proceedings of the National Meeting of JWS*, No. 66, pp. 144–145.
[11] Zhou, J., Tsai, H. L., and Wang, P. C., 2006, "Transport Phenomena and Keyhole Dynamics During Pulsed Laser Welding," ASME J. Heat Transfer, **128**(7), pp. 680–690.
[12] Kothe, D. B., Mjolsness, R. C., and Torrey, M. D., 1991, "Ripple: A Computer Program for Incompressible Flows With Free Surfaces," LA-12007-MS, Los Alamos National Laboratory.
[13] Chiang, K. C., and Tsai, H. L., 1992, "Shrinkage-Induced Fluid Flow and Domain Change in Two-Dimensional Alloy Solidification," Int. J. Heat Mass Transfer, **35**, pp. 1763–1769.
[14] Miyamoto, I., Ohmura, E., and Maede, T., 1997, "Dynamic Behavior of Plume and Keyhole in CO_2 Laser Welding," in *Proceedings of the ICALEO*, Sec. G, pp. 210–218.
[15] Dowden, J., Postacioglu, N., Davis, M., and Kapadia, P., 1987, "A Keyhole Model in Penetration Welding WIth a Laser," J. Phys. D, **20**, pp. 36–44.
[16] Siegel, R., and Howell, J. R., 1992, *Thermal Radiation Heat Transfer*, 3rd ed., Hemisphere, NY, Chap. 13.
[17] Wang, Y., and Tsai, H. L., 2001, "Impingement of Filler Droplets and Weld Pool Dynamics During Gas Metal Arc Welding Process," Int. J. Heat Mass Transfer, **44**, pp. 2067–2080.